Long/Short-term Research Visit

2023LS-08

Disaster Prevention Research Institute

Kyoto University

The Impact of Climate Change on Precipitation Extremes Across East Asia and Japan

March, 2023

Coordinator Gan Thian Yew

The impact of climate change on precipitation extremes across East Asia and Japan

Jin Zhao[1], Thian Yew Gan[1,2], Takahiro Sayama[2], Kai Ernn Gan[3], Zhang[4], S., and Zhang[5], G.,

[1]*Department of Civil and Environmental Engineering, University of Alberta, Canada*
[2]*Disaster Prevention Research Institute, Kyoto University, Kyoto, Japan*
[3]*Department of Computer and Electrical Engineering, University of Alberta, Canada*
[4]*School of Environmental Science and Engineering, Southern University of Science and Technology, Shenzhen, China*
[5]*College of Hydraulic Science & Engineering, Yangzhou University, Yangzhou 225009, China*

Abstract
We investigated the impact of climate change on precipitation extremes across East Asia, particularly Japan, by evaluating selected extreme precipitation indices defined by the Expert Team on Climate Change Detection and Indices (ETCCDI) using historical simulations (1981-2010) of 22 Global Climate Models (GCMs) of the sixth Coupled Model Intercomparison Project (CMIP6), and reanalysis dataset of the Japanese 55-year (JRA-55), the National Centers for Environmental Prediction (NCEP) and National Center for Atmospheric Research (NCAR) NCEP-NCAR, and ERA5. The CMIP6 multi-model ensemble median (CMIP6-EnM) can generally capture the extreme precipitation patterns of East Asia and Japan, could reproduce historical spatial patterns of precipitation events, and it out-performs all 22 individual GCMs of CMIP6 with a smaller normalized $RMSE'_{XY}$. Over 1958-2014, East Asia has experienced significant warming especially in high latitude areas (over 3°C in the Arctic), but drying trends limited only to some parts of Asia. Japan has experienced relatively modest warming trends by about 0.2-0.3°C partly because it is surrounded by water. Over 1958-2014, East Asia and Japan had generally experienced drying trends between 1960s and 1990s, but from 1990s onwards, Japan has been experiencing wetting trends. In general, historical changes in extreme precipitation events based on the NCEP-NCAR reanalysis data are larger than JRA-55 reanalysis data, but changes based on both datasets are larger than that of CMIP6-EnMedian because of the averaging effect of using the median of simulations of GCMs of CMIP6. Under climate warming, Japan will likely become wetter, but changes will likely be less than the increase in atmospheric water vapor expected at about 7%/°C (Clausius Clapeyron scaling).

Key words
Extreme precipitation indices, Global Climate Models simulations, CMIP6, reanalysis data, climate warming, East Asia, and Japan

1. Introduction

Since the beginning of industrial revolution (IPCC, 2018), global warming has affected the climate worldwide, including Asia, with a higher degree of warming in northern latitudes, especially in the Arctic where the annual temperature has increased by over 3°C in the last several decades, commonly known as Arctic amplification (Rantenan et al., 2022; Serreze and Barry, 2011). Associated with climate warming are higher specific humidity and potential ET, and a wide range of changes to precipitation and surface runoff worldwide (Connors et al., 2021). Based on our understanding of the coupling between the global energy and water budgets, an increase in global mean evaporation and precipitation in response to an increase in global mean surface temperature alone would be about 2-3 % per °C, even though the actual rate is less, very likely 1-2.5 % per °C due to the rapid atmospheric response to the vertical profile of atmospheric heating by greenhouse gases GHGs and anthropogenic aerosols, which reduce global precipitation and alter large-scale atmospheric circulation patterns through their surface radiative cooling effect. Land use and land cover changes also drive regional water cycle changes through their influence on land surface water and energy budgets (Douville et al., 2021).

The water cycle variability and related extremes are projected to increase in most regions of the world. Subjected to uncertainties, the interannual variability of precipitation over land is generally expected to increase faster than changes in the seasonal mean precipitation amount. Intra-seasonal precipitation variability is also projected to increase with fewer rainy days but increased daily mean precipitation intensity over many land regions. Percentage changes in precipitation extremes are projected to predominantly increase, even where seasonal mean precipitation is projected to decrease, and more pronounced than collocated changes in mean precipitation intensity (Douville et al., 2021). Global warming will also generally increase the seasonality of precipitation, with larger contrast between wet and dry seasons.

2. Extreme Precipitation Indices

Following the Expert Team on Climate Change Detection and Indices (ETCCDI), ten precipitation indices are analyzed in this study, which can be grouped under the following basic categories:

(1) Consecutive Dry Days (CDD) is the maximum length of dry spell, maximum number of consecutive days with the daily precipitation amount on a wet day, RR < 1mm, while Consecutive Wet Days (CWD) is the maximum length of wet spell, maximum number of consecutive days with RR ⩾ 1mm.
(2) PRCPTOT is the annual total precipitation in wet days with the daily precipitation amount RR ⩾ 1mm.
(3) R95p is the 95th percentile of precipitation on wet days when the daily precipitation amount RR ⩾ 1.0mm in the study period while R99p is the 99th percentile of precipitation on wet days in the study period.
(4) Rx1day is the maximum 1-day and Rx5day is the consecutive 5-day precipitation for both annual and monthly time scales.
(5) R10mm is the annual count of days when PRCP⩾ 10mm while R20mm is the annual count of days when PRCP⩾ 20mm.
(6) SDII is the simple precipitation intensity index

Equations to compute the above ETCCDI precipitation indices are presented in Table 2 (Karl et al., 1999; Peterson et al., 2001).

High values of Rx1day could result in flash floods expected to cause damages and hazards to municipal infrastructure, transportation networks, and others, while high Rx5day could lead to large-scale river flooding, resulting in extensive and long-term damages, leading to

considerable damage not only to infrastructure and property but also to human lives (Kirchmeier-Young and Zhang, 2020).

3. Global Climate Models

A global climate or circulation model (GCM) is a three-dimensional computer model of Earth's air-land-water system. A GCM simulates the state of the atmosphere and general atmospheric circulations driven by internal, potential (radiative, conductive, and latent heat) and kinetic energy (Washington and Parkinson, 1986). It also simulates atmospheric, gravity and planetary waves, geostrophic motion, convection, etc., using the Equation of Motion (continuity equation), climate variables of the climate system –temperature, precipitation, humidity, and atmospheric pressure. In essence, as a GCM describes key components, processes, and interactions in the Earth's climate system. It considers global energy and water fluxes: short and longwave radiation, atmospheric water vapor, precipitable water, geopotential, clouds, and many other climate variables at certain spatial and temporal resolutions. Using mainframe and supercomputers, GCMs simulate how changes in the flow of energy, water fluxes and atmospheric pressure affect the present climate system. GCMs have also been used extensively to project future climate under the impact of global warming. They are also coupled atmospheric-ocean general circulation models (AOGCMs) that simulate atmosphere-ocean interactions (McGuffie and Henderson-Sellers, 2014).

Simulations of GCMs are validated against observations to see if the models correctly simulate what had happened in the past. If the model accurately simulates past observations, such as temperature and precipitation trends, change points, etc., we will be more confident about GCMs' projections of future climate, but always with some degree of uncertainties. With increased spatial resolutions and more realistic parameterization schemes of GCMs over the last several decades, the recent increase in scientific knowledge and computer capability has led to greater accuracy in climate models used by the Intergovernmental Panel on Climate Change (IPCC). The recent IPCC sixth assessment report, known as AR6, compared results of over 40 different GCMs to make predictions about the future climate. In this study, the climate projections of 22 GCMs of CMIP6 (Coupled Model Inter-comparison Project #6) of IPCC are selected to investigate the impact of climate change to East Asia and Japan (Table 1).

4. Study Site

East Asia which includes Japan is selected for this study, to investigate the impact of climate change to inlands of East Asia and Japan surrounded by the Sea of Japan and the Pacific Ocean. Asia, defined as the land of 51 countries/regions, can be broadly divided into six sub-regions based on geographic position and coastal peripheries (IPCC, 2014), which are Central Asia (5 countries), East Asia (7 countries), North Asia (2 countries), South Asia (8 countries), Southeast Asia (12 countries) and West Asia (17 countries) (Shaw et al., 2022).

GHG forcing has driven increased contrasts in precipitation amount between wet and dry seasons in many regions, earlier onset of spring snowmelt, melting of glaciers and higher runoff in high latitudes due to higher precipitation amount and intensity, but increased evapotranspiration due to growing atmospheric water demand will result in lower soil moisture in summer-midlatitude areas (Douville et al., 2021; Lee et al., 2021).

Since the early 20th century all over Asia significant warming has intensified the threat to social and economic sustainability (Shaw et al., 2022). Higher temperatures increase the possible threat of heatwaves across Asia, droughts in arid and semiarid regions of South, West, and Central Asia, weakened and delayed monsoon circulation in South Asia, flooding in monsoon regions in Southeast, East and South Asia, and glacier melting in the Hindu Kush Himalaya region. Very likely the greatest challenge to Asia will be increasing surface air temperature especially along the higher latitudes of North Asia, rise in nighttime temperature, and multiple

observed changes to monsoon rainfall variability, seasonally, interannually and spatially; upwards trend in the intensity and frequency of extreme weather events; and worsening flood risks (Hijioka et al., 2014).

Terrestrial ecosystems of Asia are changing, driven by global warming, precipitation and Asian monsoon alteration, permafrost thawing and extreme events such as dust storms. Asian countries are experiencing hotter summers and lower precipitation. Climate change has caused damage in infrastructure, disruption in services and affected supply chains in Asia and will increase risk to infrastructure malfunction. As Asia is a vast continent, it is beyond the scope of this report to provide a detailed discussion for the whole continent. Therefore we will focus on recent changes to the extreme precipitation of East Asian, and especially Japan.

5. Climate of East Asia and Japan

We consider examining the general climatology of East Asia of 1950-2020 using several sets of reanalysis data such as the NCEP-NCAR, ERA5, JRA-55 and APHRODITE (Asian Precipitation-Highly Resolved Observational Data Integration Toward Evaluation). Figure 1 shows the air temperature, specific humidity and precipitation rate of East Asia using NCEP-NCAR, ERA5, and JRA-55 reanalysis data. Overall, East Asia has been getting warmer and more humid in the last seven decades, increasing at slightly more than 0.01^{o}C/year, higher specific humidity at 0.004-0.007 g/g per year, and higher precipitation rate ($\approx$ 0.003mm/day/year).

The mean (changes) annual climate of East Asia over 1948-2018 (between 1983-2018 and 1948-1982) is further examined in terms of air temperature (^{o}C), surface precipitable water (kg/m^2), GPCP precipitation (mm/day), soil Moisture (mm), specific humidity (g/kg), and the Palmer Drought Severity Index of East Asia (Figure 2). Overall, East Asia has become progressively warmer in the last forty years, from about 0.2-0.3^{o}C in South East Asia, South China Sea, to about 1.5^{o}C in high latitude regions of Siberia, to as much as 3-4^{o}C in the high Arctic. In contrast, precipitation has marginally decreased by about 1 mm/day in Japan but marginally increased near Philippines (up to 1.5 mm/day), which combined with an increase in potential ET by about 10 to 20 W/m^2 or 10-20mm, except a marginal decrease in India and south central China, resulting in marginally less surface runoff across large parts of East Asia though there are also marginal increase in India and parts of central Asia (Supplementary Figure S1). Changes to the Palmer Drought Severity Index are predominantly marginal except in the Middle East, and north eastern China, up to -2 which means significantly drier climate in these regions. Specific humidity has increased marginally in the south but decreased in East China and Japan even though climate warming should generally gives rise to more atmospheric humidity by about 6-7% per ^{o}C of warming. There has been minimal overall changes to the precipitable water except in eastern China and Mongolia where precipitable water has decreased by about 0.5 to 1 kg/m^2, and minimal changes to the surface runoff which has either marginally increased or decreased by $\pm$ 0.5 kg/m^2.

The climate of Japan and recent changes are shown in Figures 3 and 4. The average annual air temperature of Japan ranges from about 18^{o}C in the south to about 7^{o}C in the north, while the annual average daily precipitation ranges from about 5mm/day in the south to about 3 mm/day in the north Island of Hokkaido. Japan has also been getting marginally warmer over the last forty years since 1980 by about 0.2 to 0.3^{o}C, in contrast to eastern China which has experienced considerably higher warming by up to 1^{o}C. It seems climate change impact is less severe in Japan compared to China or other parts of the world partly because Japan is surrounded by oceans. Changes to the annual daily precipitation of Japan has been minimal, generally within 0.1 mm/day over the last forty years. Its geopotential height has somewhat decreased, by up to 3 m since 1980s. The average annual geopotential height decreases from about 130m in the south to about 100m in the northern part of Hokkaido (Figure 4).

Changes of annual air temperature, specific humidity, precipitable water and precipitation rate of Japan of 1948-2022 using NCEP-NCAR reanalysis data are presented in Figures 3a-3d. Japan experienced consistent warming trends since 1960s, became somewhat drier between 1948 and mid-1970s, but wetter again thereafter (higher specific humidity). However, the precipitable water and precipitation rate fluctuated for about two decades (1970-1990s) before showing consistent increasing trends since the beginning of the 21st Century. Figure 3e shows that the seasonal mean precipitation over regional monsoon domains of East Asia is projected to increase for 2020s, 2050s, and 2080s based on 24 CMIP6 models and three SSP scenarios (SSP1-2.6, SSP2-4.5 and SSP5-8.5). Figure 3f shows projected increasing trends (%) in seasonal mean total precipitable water, precipitation, runoff in summer (JJA) as a function of global-mean surface temperature for the CMIP6 multi-model mean across the SSP5-8.5 scenarios.

Next, in view of such climatic changes observed across East Asia and Japan (Figures 2 and 4), we also conducted more detailed investigations on changes to extreme precipitation events of Japan over 1958-2014 using reanalysis data and CMIP6 Global climate Models' simulations for the historical period.

5. Performance of Global Climate Models of CMIP6

The performance of CMIP6 GCMs has been evaluated in various studies using the root mean squared error (RMSE) statistics at both global and regional scales (Kim et al., 2020; Sillmann et al., 2013a; A. Srivastava et al., 2020; Xu et al., 2019). The annual, spatially-averaged extreme precipitation indices simulated by GCMs are evaluated against corresponding statistics of reanalysis (NCEP-NCAR) and observed datasets (JRA-55) for 1981-2010 using defined as:

$$RMSE_{XY} = \sqrt{< (X - Y)^2 >} \quad (1)$$

where X and Y represent the extreme precipitation index estimated from the simulations of a GCM of CMIP6 and that estimated from the observed dataset at a grid point, respectively. The angular brackets represent the mean for all grids points over Japan. $RMSE'_{XY}$ is the normalized RMSE that evaluates the performance of GCMs of CMIP6 with respect to observations. is defined as:

$$RMSE'_{XY} = \frac{RMSE_{XY} - RMSE_{Median}}{RMSE_{Median}} \quad (2)$$

where $RMSE_{Median}$ is the median of an index for 22 GCMs of CMIP6 (excluding CMIP6-EnM).

Results show that CMIP6-EnM could well reproduce the historical spatial patterns of observed precipitation events over East Asia. As expected, northern East Asia tends to be drier than southern East Asia and Japan that is surrounded by the Sea of Japan in the west, South China Sea in the south and the Pacific Ocean in the east, respectively. Therefore, moving from north to south and from inlands to coastal regions, all extreme precipitation indices (except CDD) tend to increase. Further, the spatial patterns of these indices are generally similar to each other. Only CDD has a spatial pattern that is opposite, that decreases moving south and towards the seas.

6. Reanalysis data and simulations of Global Climate Models of CMIP6 for Japan

The Japanese 55-year Reanalysis (C) data was updated by the Japan Meteorological Agency to overcome deficiencies of the Japanese 25-year Reanalysis to provide a long-term, more comprehensive atmospheric dataset. In JRA-55, a higher spatial resolution, a new radiation

scheme in the forecast model and the 4D-Var with variational bias correction were adopted, and the application of additional satellite observations. Further, JRA-55 includes greenhouse gases of time-varying concentrations to improve the data quality and provide data from 1958 to present. JRA-55 data is given at http://jra.kishou.go.jp/JRA-55/index_en.html.

NCEP-NCAR is a global reanalysis data developed by The National Centers for Environmental Prediction (NCEP) and the National Center for Atmospheric Research (NCAR). It provides 4-times daily, daily and monthly weather data with the global grids of 2.5 degree × 2.5 degree from 1948 to present. In this study, daily precipitation data was download at https://psl.noaa.gov/data/gridded/data.ncep.reanalysis.html

We compared the above reanalysis data with the historical runs of 22 GCMs of CMIP6 from 1958 to 2014 relative to 1981-2010 with details of the GCMs listed in Table 1 below. The comparisons are based on twelve extreme precipitation indices shown in Table 2. The percentage of linear trends of JRA-55, NCEP-NCAR and CMIP6-EnMedian for the 12 extreme precipitation indices over the 1958–2014 study period are shown in Figure 5, where increasing and decreasing trends are shown in red and blue, respectively.

7. Global Climate Model performance metrics

The portrait diagram in Figure 6 provides an assessment of the performance of 22 CMIP6-GCMs in simulating twelve extreme precipitation indices of ETCCDI such as CDD, CWD, PRCPTOT, R10mm, etc., with reference to the reanalysis dataset JRA-55. Negative (Positive) values shown in blue (red) indicate that the GCM performs better (poorer) than the majority (50%) of selected GCMs. The assessment results in the simulations of GCMs assume that the observed dataset is correct even though observed data inevitably has some uncertainty due to the limitations of point measurements of climate stations and converting point measurements of climate stations to gridded data. GCMs such as NorESM2-LM and NorESM2-MM, perform relatively well, with the most negative $RMSE'_{XY}$ in Figure 6. In contrast, INM-CM4-8 and INM-CM5-0 show relatively weak performances with high positive values, especially for CWD, PRCPTOT, R10mm, R20mm, R95p and R99p. However, CMIP6-EnM show negative $RMSE'_{XY}$ for all indices, indicating that the CMIP6-EnM is more robust than precipitation events simulated by individual GCMs in Japan because as the median at each grid interpolated from the simulations of 22 CMIP6 models over the grids of Japan, CMIP6-EnM could cancel some of the simulation errors (either over or under simulations) in individual climate models.

To better understand the temporal changes of these precipitation indices, the relative change of the twelve indices estimated from the JRA-55 and NCEP-NCAR reanalysis data, and that of CMIP6-EnMedian between 1960 and 2010 are analyzed. Figure 7 shows that both reanalysis datasets JRA-55 and NCEP-NCAR generally give higher positive or negative trends compared to the CMIP6 Ensemble Median because of the averaging effect of using the median of 22 sets of GCMs' simulations, of which some represent over-simulations while some under-simulations. Among the twelve indices, some show increasing trends while others show decreasing trends. For example, CDD, R95p, R95ptot, R99p and R99pot generally show increasing trends across Japan while CWD and R10mm show decreasing trends, and R20mm show both increasing and decreasing trends across Japan. It seems Japan has experienced both dryer and wetter climate over the study period of 1958-2014.

The results computed from the NCEP-NCAR dataset generally show larger changes compared to that of JRA-55, but that of CMIP6-EnMedian generally show temporal fluctuations with little clear indications of positive or negative trends in many of the twelve precipitation indices estimated (Figure 7). Interestingly, based on results obtained from both reanalysis datasets, Japan experienced a short period of dry spells between late 1980s and early 1990s as distinctly

shown by the time series of all the twelves indices estimated from both reanalysis datasets, which could be linked to the influence of La Nina episodes of late 1980s. More in-depth analysis is needed to confirm the reasons behind these brief drying episodes over Japan.

Changes of Precipitation Extremes in Japan over 1958-2014 based on selected extreme precipitation indices defined by the Expert Team on Climate Change Detection and Indices (ETCCDI) are evaluated over the four large islands of Japan: Hokkaido, Honshu, Shikoku, and Kyushu using the simulations of 22 Global Climate Models (GCMs) of the sixth Coupled Model Intercomparison Project (CMIP6), the Japanese 55-year (JRA-55), and the National Centers for Environmental Prediction (NCEP) and National Center for Atmospheric Research (NCAR) NCEP-NCAR, and ERA5 reanalysis data. The temporal variations, spatial distributions, and seasonal patterns of precipitation extremes over 1958-2014 relative to 1981-2010, are based on the selected extreme precipitation indices, which show that Japan had generally experienced drying trends between 1960s and 1990s, but from 1990s onwards, Japan has been experiencing wetting trends. In general, historical changes in extreme precipitation events based on the NCEP-NCAR reanalysis data are larger than JRA-55 reanalysis data, but changes based on both datasets are larger than that of CMIP6-EnMedian which is expected because of the averaging effect from using the median of simulations of 22 GCMs of CMIP6 (Figure 7). Under the effect of warming, the climate of Japan will likely become wetter because the atmospheric water vapor is expected to increase at about 7% per degree of warming (Clausius Clapeyron scaling).

Taylor diagrams of ten extreme precipitation indices between observation and 35 CMIP6-GCMs over East Asia (Figure 8) show that the correlation between observation and simulations of extreme precipitation by these CMIP6-GCMs varies from about 0.75 for CWD to 0.95 for PRCPTOT which is statistically significant at 95% significant level, which demonstrates the consistency of GCMs' simulations on spatial and temporal patterns of extreme precipitation over East Asia. Figure 9 shows spatial distributions of extreme precipitation indices over East Asia and Japan based on the ensemble median of CMIP6 GCMs' simulations for 1958-2014 (CMIP6-EnM). Supplementary

Figure 10 shows some limited correlation between precipitation of East Asia with the EOF of Tropical Pacific SST but the correlation is season dependent, predominantly negative in the summer (Figure 10a) but positive in the winter (Figure 10b). The precipitation of East Asia (especially Japan) is predominantly negatively correlated with ENSO (Figure 10c), which means less precipitation when El Nino is active but more precipitation when La Nina is active, similar to the effect of ENSO to the precipitation of western Canada (Gan et al., 2007). The precipitation of East Asia is somewhat marginally correlated with the Western Pacific Index (WP), but the correlation could either be positive or negative (Figure 10d).

8. Projected Climate Change Impact to Extreme Precipitation of East Asia

The ensemble medians of projected changes to eight extreme precipitation indices (CWD, CDD, R95p, R99p, Rx1day, Rx5day, PRCPTOT, and SDII) of East Asia under SSP1-2.6, SSP2-4.5 and SSP5-8.5 climate scenarios of CMIP6-GCMs (8 GCMs) for the 2050s and 2080s are presented in Figure 11. Figure S2 shows the corresponding projected changes to East Asia of CMIP6-GCM CESM2.

Overall, there are more severe projected changes in CWD in northern East Asia, but more severe projected changes in CDD in southern East Asia, especially in 2080s. As expected, severity of projected changes in R95p and R99p increase from SSP1-2.6 to SSP5-8.5, especially in 2080s, given atmospheric humidity increases at $\approx$ 7%/^{o}C of warming. Severity of projected changes in Rx1day and Rx5day are less compared to that of R95p and R99p from SSP1-2.6 to

SSP5-8.5 given projected changes in maximum 1-day and 5-day precipitation should be less than changes in annual total precipitation of R95p and R99P under climate change impact. Annual total precipitation in wet day (PRCPTOT) and precipitation intensities (SDII) are both projected to increase more in northern than in southern Asia, given projected changes in precipitation are expected to increase with latitudes under warming impact (Douville et al., 2021).

9. Uncertainties of Climate Change Projections

A quantitative assessment of the uncertainty components of future climate projections is critical for decision-makers and organizations to establish robust climate change adaptation and mitigation strategies at regional or local scales. Over East Asia, Park et al. (2024) quantitatively evaluated changes in the uncertainty components of future temperature and precipitation projections using multiple regional climate models. For temperature, internal variability and model uncertainty were the main factors affecting the near-term projections. The scenario uncertainty continued to increase and was estimated to be the dominant factor affecting the uncertainty after the mid-term projections (Kirtman et al., 2013). Although precipitation has the same main uncertainty factors as the temperature in the near-term projections, it considerably differs from temperature because the internal variability notably contributes to the fraction to the total variance, even in the long-term projections. The internal variability of the temperature and precipitation in the near-term projections were predicted to be larger in Korea than that in East Asia, confirmed by regional and global climate models regarding the importance of internal variability at smaller regional scales during the near-term projections.

10. Summary and Conclusions

On the basis of the results obtained from the 10 ETCCDI extreme precipitation indices analyzed, the CMIP6 multi-model ensemble median (CMIP6-EnM) out-performs all 22 individual GCMs with negative $RMSE'_{XY}$ over East Asia (Figure 2), the signal-to-noise ratio (SNR) > 1 (Figure 3) in most sub-regions. Therefore, CMIP6-EnM could reasonably reproduce the spatial patterns of observed precipitation events. East Asia has experienced significant warming especially in high latitude areas, but drying trends limited only to some parts of Asia attributed to higher potential evapotranspiration and are relatively modest. Since 1980s, Japan has experienced relatively modest warming trends compared to other parts of the world by about 0.2-0.3^{o}C of warming in the last several decades because it is surrounded by water. It has also experienced both drying and wetting trends over this period.

Changes of Precipitation Extremes in Japan over 1958-2014 based on twelve extreme precipitation indices of ETCCDI are evaluated over the four large islands of Japan: Hokkaido, Honshu, Shikoku, and Kyushu based on the simulations of 22 Global Climate Models (GCMs) of CMIP6, the Japanese 55-year (JRA-55), and the National Centers for Environmental Prediction (NCEP) and National Center for Atmospheric Research (NCAR) NCEP-NCAR reanalysis data. The temporal variations, spatial distributions, and seasonal patterns of precipitation extremes over 1958-2014 relative to 1981-2010, are based on the twelve extreme precipitation indices, which show that Japan had generally experienced drying trends between 1960s and 1990s, but from 1990s onwards, Japan has been experiencing wetting trends. In general, historical changes in extreme precipitation events based on the NCEP-NCAR reanalysis data are larger than JRA-55 reanalysis data, but changes based on both datasets are larger than that of CMIP6-EnMedian which is expected because of the averaging effect from using the median of simulations of 22 GCMs of CMIP6. Under the effect of warming, the climate of Japan will likely become wetter, but the changes will likely be less than the increase in atmospheric water vapor expected at about 7% per degree of warming (Clausius Clapeyron scaling).

In summary:

(1) Extreme precipitation indices (EPI) estimated using JRA-55 and ERA5 reanalysis data show more changes over 1958-2014 than that of CMIP6-Median Ensemble, which is possibly due to the averaging effects of simulations of CMIP6 GCMs.
(2) Based on most EPI estimated from JRA-55 and ERA5 data, Japan experienced a relatively dry period in 1980-1995, that southern Japan has become marginally wetter but northern Japan marginally drier.
(3) Ten extreme precipitation indices estimated from SSP climate projections, SSP1-2.6, SSP2-4.5 and SSP5-8.5 of the eight CMIP6 GCMs are R95p, R99p, Rx1day, Rx5day, PRCPTOT, SDII, CDD, CWD, R10mm, and R20mm. Statistically significant correlation between Taylor diagrams and IVS (Inter-annual Variability Skill Score) for extreme precipitation show the consistency of 35 CMIP6 GCMs' simulations on spatial and temporal patterns (Supplementary figures S3 and S4).
(4) More severe projected changes in CWD (CDD) in northern (southern) East Asia, especially in 2080s. Severity of projected changes in R95p and R99p increase from SSP1-2.6 to SSP5-8.5, for atmospheric humidity is expected to increase at $\approx$ 7%/^{o}C in warming - Claudius Clapeyron Scaling. Severity of projected changes in Rx1day and Rx5day are less compared to that of R95p and R99p from SSP1-2.6 to SSP5-8.5 given projected changes in maximum 1-day and 5-day precipitation should be less than changes in the annual total precipitation of R95p and R99p under the effect of climate warming.
(5) Annual total precipitation in wet day PRCPTOT and precipitation intensities SDII are both projected to increase more in northern than in southern East Asia, given projected changes in precipitation are generally expected to increase with latitudes under warming.
(6) Precipitation of East Asia or Japan could be affected by climate patterns such as El Niño Southern Oscillations and Western Pacific Index (WP).

Acknowledgements
This study was partly funded by the Disaster Prevention Research Institute of Kyoto University of Japan, the University of Alberta, Canada, and Japan Society of Promotion of Science.

References

Connors, S., S. Berger, C. Péan, G. Bala, N. Caud, D. Chen, T. Edwards, S. Fuzzi, T. Y. Gan, M. Gomis, E. Hawkins, R. Jones, R. Kopp, K. Leitzell, E. Lonnoy, D. Maraun, V. Masson-Delmotte, T. Maycock, A. Pirani, R. Ranasinghe, J. Rogelj, A. C. Ruane, S. Szopa, and P. Zhai, 2021,*Climate Change 2021, Summary For All*, Working Group I to the Sixth Assessment Report of the Intergovernmental Panel on Climate Change.

Douville, H., Krishnan, R., Renwick, J., Allan, R., Arias, P., Barlow, M., CerezoMota, R., Cherchi, A., Gan, T. Y., J. Gergi, D. Jiang, A. Khan, W. P. Mba, D. Rosenfeld, J. Tierney, O. Zolina, 2021, Water Cycle Change, *In: Climatic Change, 2021: the physical science basis*. Contribution of Working Group I to the Sixth Assessment Report of the Intergovernmental Panel on Climate Change, Masson-Delmotte, et al., (Eds.). Cambridge, UK: Cambridge University Press.

Hijioka, Y., E. Lin, J.J. Pereira, R.T. Corlett, X. Cui, G.E. Insarov, R.D. Lasco, E. Lindgren, and A. Surjan, 2014: Asia, In: Climate Change 2014: Impacts, Adaptation, and Vulnerability. Part B: Regional Aspects. Contribution of Working Group II to the *Fifth Assessment Report of the Intergovernmental Panel on Climate Change* [Barros, V.R., C.B. Field, D.J. Dokken, M.D. Mastrandrea, K.J. Mach, T.E. Bilir, M. Chatterjee, K.L. Ebi, Y.O. Estrada, R.C. Genova, B. Girma, E.S. Kissel, A.N. Levy, S. MacCracken, P.R. Mastrandrea, and L.L.White (eds.)]. Cambridge University Press, Cambridge, UK and NY, USA, pp. 1327-1370.

IPCC, 2018, Global Warming of 1.5°C, an IPCC Special Report on the impacts of global warming of 1.5°C above pre-industrial levels and related global greenhouse gas emission pathways, in the context of strengthening the global response to the threat of climate change, sustainable development, and efforts to eradicate poverty [Masson-Delmotte, V., P. Zhai, et al., (eds.)]

Karl, T.R., N. Nicholls, and A. Ghazi, 1999: CLIVAR/GCOS/WMO workshop on indices and indicators for climate extremes: Workshop summary. Climatic Change, 42, 3-7.

Keywan, Riahi; van Vuuren, Detlef P.; Kriegler, Elmar; Edmonds, Jae; O'Neill, Brian C.; Fujimori, Shinichiro; Bauer, Nico; Calvin, Katherine; Dellink, Rob; Fricko, Oliver; Lutz, Wolfgang, 2017, The Shared Socioeconomic Pathways and their energy, land use, and greenhouse gas emissions implications: An overview, Global Environmental Change. 42: 153–168. doi:10.1016/j.gloenvcha.2016.05.009. ISSN 0959-3780.

Kim, Y.-H., Min, S.-K., Zhang, X., Sillmann, J., & Sandstad, M. (2020). Evaluation of the CMIP6 multi-model ensemble for climate extreme indices. *Weather and Climate Extremes*, *29*, 100269. https://doi.org/10.1016/j.wace.2020.100269

Kirtman, B., S.B. Power, J.A. Adedoyin, G.J. Boer, R. Bojariu, I. Camilloni, F.J. Doblas-Reyes, A.M. Fiore, M. Kimoto, G.A. Meehl, M. Prather, A. Sarr, C. Schär, R. Sutton, G.J. van Oldenborgh, G. Vecchi and H.J. Wang, 2013, Near-term Climate Change: Projections and Predictability. In: *Climate Change 2013: The Physical Science Basis,* Contribution of WGI to the AR5 of the Intergovernmental Panel on Climate Change [Stocker, T.F., D. Qin, G.-K. Plattner, M. Tignor, S.K. Allen, J. Boschung, A. Nauels, Y. Xia, V. Bex and P.M. Midgley (eds.)]. Cambridge University Press, Cambridge, UK and NY, USA.

Lee, J.Y., J. Marotzke, G. Bala, L. Cao, S. Corti, J. Dunne, F. Engelbrecht, E. Fischer, J. Fyfe, C. Jones, A. Maycock, J. Mutemi, O. Ndiaye, S. Panickal, and T. Zhou, 2021, Future global climate: scenario-based projections and near-term information, *In: Climatic Change, 2021: the physical science basis*. Contribution of WGI to AR6 of the Intergovernmental Panel on Climate Change, Masson-Delmotte, et al., (Eds.), CUP.

McGuffie, K., and A. Henderson-Sellers, 2014, *The Climate Modelling Primer*, 4th Edition, 439 pgs., Wiley Blackwell.

Park, C., Shin, SW., Juzbašić, A. et al., 2024, Uncertainty assessment of future climate change using bias-corrected high-resolution multi-regional climate model datasets over East Asia. *Clim Dyn*, 62, 1983–1996 (2024). https://doi.org/10.1007/s00382-023-07006-z

Peterson, T.C., and Coauthors, 2001, Report on the Activities of the Working Group on Climate Change Detection and Related Rapporteurs 1998-2001. WMO, Rep. WCDMP-47, WMO-TD 1071, Geneve, Switzerland, 143pp.

Rantanen, M., Karpechko, A.Y., Lipponen, A. et al., 2022, The Arctic has warmed nearly four times faster than the globe since 1979, *Commun Earth Environ*, 3, 168, https://doi.org/10.1038/s43247-022-00498-3

Saha, S., and coauthors, 2010: The NCEP Climate Forecast System Reanalysis. *Bull. Amer. Meteor*. Soc., 91:8, 1015–1057.

Serreze, M., and Barry, R., 2011, Processes and impacts of Arctic amplification: A research synthesis, *Global & Planetary Change*, 77(1–2), doi.org/10.1016/j.gloplacha.2011.03.004

Shaw, R., Y. Luo, T.S. Cheong, S. Abdul Halim, S. Chaturvedi, M. Hashizume, G.E. Insarov, Y. Ishikawa, M. Jafari, A. Kitoh, J. Pulhin, C. Singh, K. Vasant, and Z. Zhang, 2022: Asia. In: Climate Change 2022: Impacts, Adaptation and Vulnerability. Contribution of Working Group II to the Sixth Assessment Report of the Intergovernmental Panel on Climate Change [H.-O. Pörtner, D.C. Roberts, M. Tignor, E.S. Poloczanska, K. Mintenbeck, A. Alegría, M. Craig, S. Langsdorf, S. Löschke, V. Möller, A. Okem, B. Rama (eds.)]. Cambridge University Press, Cambridge, UK and New York, NY, USA, pp. 1457–1579, https://doi:10.1017/9781009325844.012

Sillmann, J., Kharin, V. V., Zhang, X., Zwiers, F. W., & Bronaugh, D., 2013, Climate extremes indices in the CMIP5 multimodel ensemble: Part 1. Model evaluation in the present climate. *Journal of Geophysical Research Atmospheres*, 118(4), 1716–1733. https://doi.org/10.1002/jgrd.50203

Srivastava, A., Grotjahn, R., & Ullrich, P. A. (2020). Evaluation of historical CMIP6 model simulations of extreme precipitation over contiguous US regions. *Weather and Climate Extremes*, 29, 100268. https://doi.org/10.1016/j.wace.2020.100268

Tsujino, H., et al., 2018, JRA-55 based surface dataset for driving ocean–sea-ice models (JRA55-do), *Ocean Modeling*, https://doi.org/10.1016/j.ocemod.2018.07.002

Xu, K., Xu, B., Ju, J., Wu, C., Dai, H., & Hu, B. X. (2019). Projection and uncertainty of

precipitation extremes in the CMIP5 multimodel ensembles over nine major basins in China. *Atmospheric Research*, 226, 122–137. https://doi.org/10.1016/j.atmosres.2019.04.018

Washington, W. M., C. L., Parkinson, 1986, *An Introduction to Three-Dimensional Climate Modeling*, 422 pgs., Oxford University Press, Oxford.

Zhou, X., Huang, G., Wang, X., & Cheng, G. (2018). Future Changes in Precipitation Extremes Over Canada: Driving Factors and Inherent Mechanism. *Journal of Geophysical Research*: *Atmospheres*, 123(11), 5783–5803. https://doi.org/10.1029/2017JD027735

Zhao, J., Gan, T. Y., Zhang, S., and, Zhang, G., 2022, Projected Changes of Precipitation Extremes in North America using CMIP6 Multi-Climate Model Ensembles, Journal of Hydrology, https://doi.org/10.1016/j.jhydrol.2023.129598

Table 1 Selected Global Climate Models of CMIP6

S/N	Model	Organization	Nominal Horizontal Grid Size	Nominal Resolution (Lon×Lat)	Run
1	ACCESS-CM2	Commonwealth Scientific and Industrial Research Organisation and	250km	192×144	r1i1p1f1
2	ACCESS-ESM1-5	Australian Research Council Centre of Excellence for Climate System Science, Australia	250km	192×145	r1i1p1f1
3	BCC-CSM2-MR	Beijing Climate Center, China Meteorological Administration, China	100km	320×160	r1i1p1f1
4	CMCC-ESM2	Centro Euro-Mediterraneo sui Cambiamenti Climatici, Italy	100km	288×192	r1i1p1f1
5	EC-Earth3		100km	512×256	r1i1p1f1
6	EC-Earth3-Veg	EC-Earth-Consortium	100km	512×256	r1i1p1f1
7	EC-Earth3-Veg-LR		250km	320×160	r1i1p1f1
8	FGOALS-g3	Chines Academy of Sciences, China	250km	180×80	r1i1p1f1
9	GFDL-ESM4	Geophysical Fluid Dynamics Laboratory, USA	100km	288×180	r1i1p1f1
10	INM-CM4-8	nstitute for Numerical Mathematics, Russia	100km	180×120	r1i1p1f1
11	INM-CM5-0		100km	180×120	r1i1p1f1
12	IPSL-CM6A-LR	Institut Pierre-Simon Laplace, France	250km	144×143	r1i1p1f1
13	KACE-1-0-G	National Institute of Meteorological Science/Korea Meteorological Administration, Korea	250km	192×144	r1i1p1f1
14	KIOST-ESM	Korea Institute of Ocean Science & TechnologyRepublic of Korea, Korea	250km	192×96	r1i1p1f1
15	MIROC6	JAMSTEC, AORI, NIES, R-CCS, Japan	250km	256×128	r1i1p1f1
16	MPI-ESM1-2-HR	Max Planck Institute for Meteorology, Germany	100km	384×192	r1i1p1f1
17	MPI-ESM1-2-LR		250km	192×96	r1i1p1f1
18	MRI-ESM2-0	Meteorological Research Institute, Japan	100km	320×160	r1i1p1f1
19	NESM3	Nanjing University of Information Science and Technology, China	250km	192×96	r1i1p1f1
20	NorESM2-LM	NorESM climate modeling Consortium of CICERO, MET-Norway, NERSC, NILU, UiB, UiO and UNI, Norway	250km	144×96	r1i1p1f1
21	NorESM2-MM		100km	288×192	r1i1p1f1
22	TaiESM1	Research Center for Environmental Changes, Academia Sinica, Taiwan	100km	288×192	r1i1p1f1

Table 2 Extreme Precipitation Indices of ETCCDI

NO.	Label	Index Name	Index Definition	Units
1	Rx1day	Max 1 day precipitation	Let RR_{ij} be the daily precipitation amount on day i in period j. The maximum 1 day value for period j are: $Rx1day_j = \max(RR_{ij})$	mm
2	RxX5day	Max consecutive 5-day precipitation	Let RR_{kj} be the precipitation amount for the 5 day interval ending k, period j. Then maximum 5 day values for period j are: $Rx5day_j = \max(RR_{kj})$	mm
3	R10mm	Heavy precipitation days	Let RR_{ij} be the daily precipitation amount on day i in period j. Count the number of days where $RR_{ij} > 10$ mm	days
4	R20mm	Very heavy precipitation days	Let RR_{ij} be the daily precipitation amount on day i in period j. Count the number of days where $RR_{ij} > 20$ mm	days
5	CDD	Consecutive dry days	Let RR_{ij} be the daily precipitation amount on day i in period j. Count the largest number of consecutive days where $RR_{ij} < 1$ mm	days
6	CWD	Consecutive wet days	Let RR_{ij} be the daily precipitation amount on day i in period j. Count the largest number of consecutive days where $RR_{ij} > 1$ mm	days
7	R95p	Very wet days	Let RR_{wj} be the daily precipitation amount on a wet day w ($RR \geq 1$ mm) in period i and let $RR_{wn}95$ be the 95th percentile of precipitation on wet days in the 1981–2010 period. If W represents the number of wet days in the period, then: $R95p_j = \sum_{w=1}^{W} RR_{wj}$, where $RR_{wj} > RR_{wn}95$	mm
8	R99p	Extremely wet days	Let RR_{wj} be the daily precipitation amount on a wet day w ($RR \geq 1$ mm) in period i and let $RR_{wn}99$ be the 99th percentile of precipitation on wet days in the 1981–2010 period. If W represents the number of wet days in the period, then: $R99pj = \sum_{w=1}^{W} RR_{wj}$, where $RR_{wj} > RR_{wn}99$	mm
9	SDII	Simple daily intensity	Let RR_{wj} be the daily precipitation amount on wet days, w($RR \geq 1$ mm) in period j. If W represents number of wet days in j, then: $SDII_j = \frac{\sum_{w=1}^{W} RR_{wj}}{W}$	mm/day
10	PRCPTOT	Total wet-day precipitation	Let RRij be the daily precipitation amount on day i in period j. If I represents the number of days in j, then: $PRCPTOT_j = \sum_{i=1}^{I} RR_{ij}$	mm
11	R95ptot	Contribution from very wet days	$R95ptot_j = \frac{R95p_j}{PRCPTOT_j}$	%
12	R99ptot	Contribution from extremely wet days	$R99ptot_j = \frac{R99p_j}{PRCPTOT_j}$	%

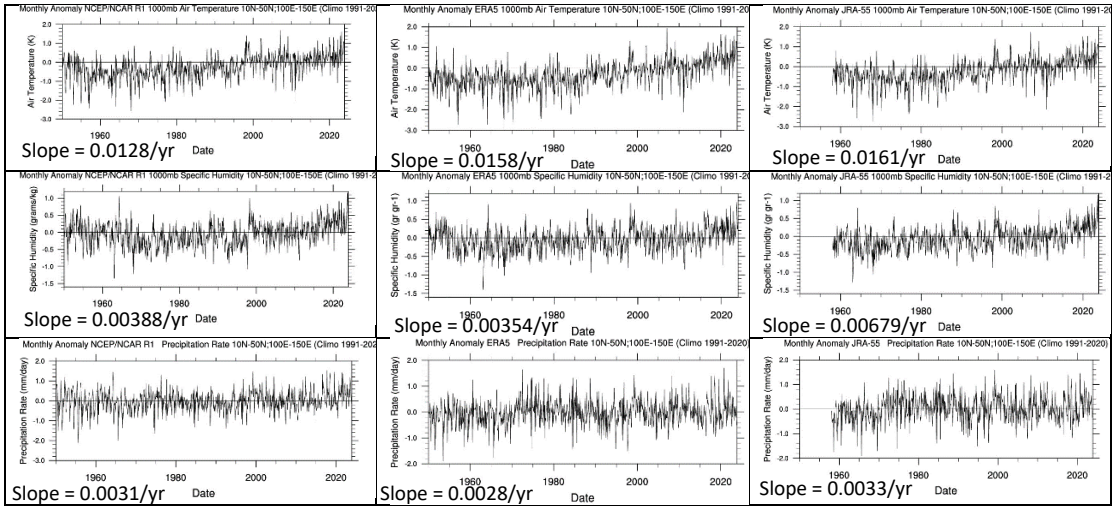

Figure 1 Monthly anomalies for summer (Jun-Sep) air temperature, specific humidity, and precipitation rate over East Asia (10-50ºN, 100-150ºE) for 1950-2020 using the reanalysis data of NCEP-NCAR, ERA5 and JRA-55, respectively, which all show consistent but modest rising trends.

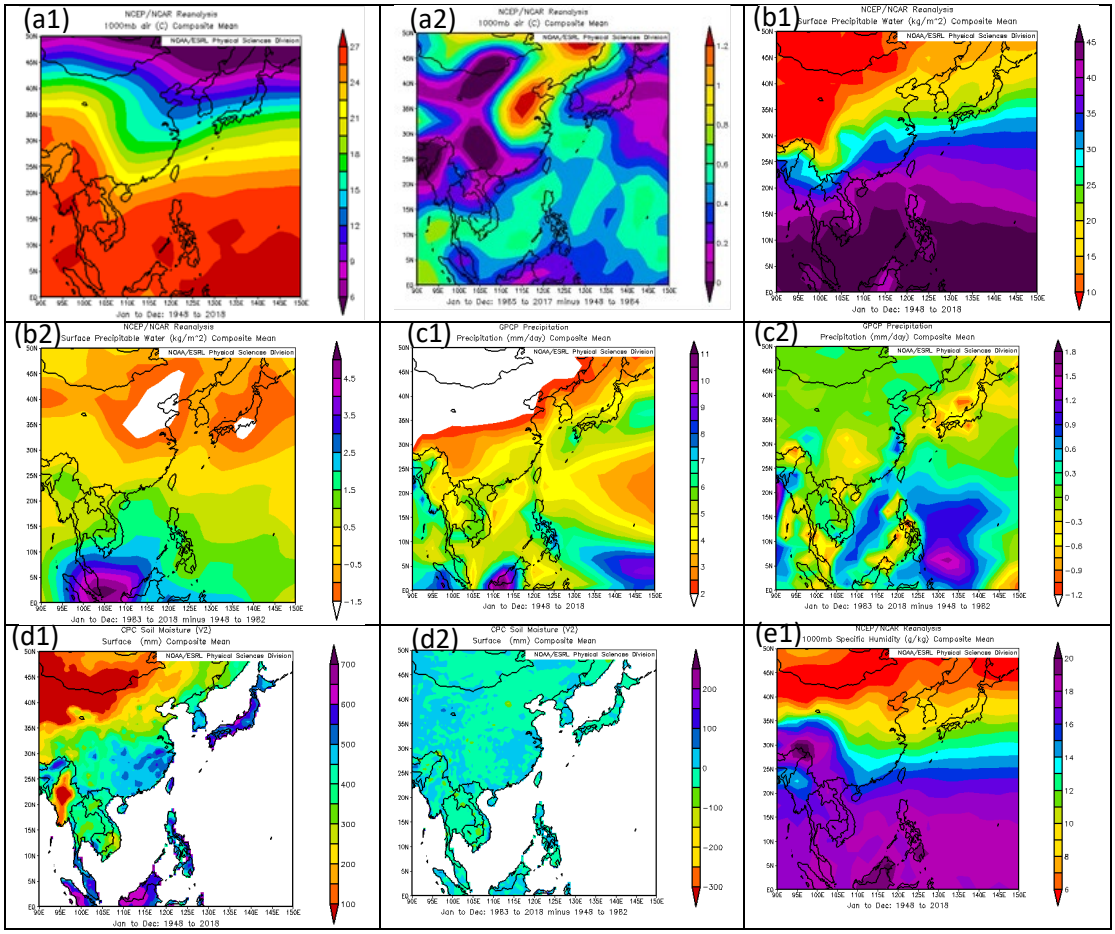

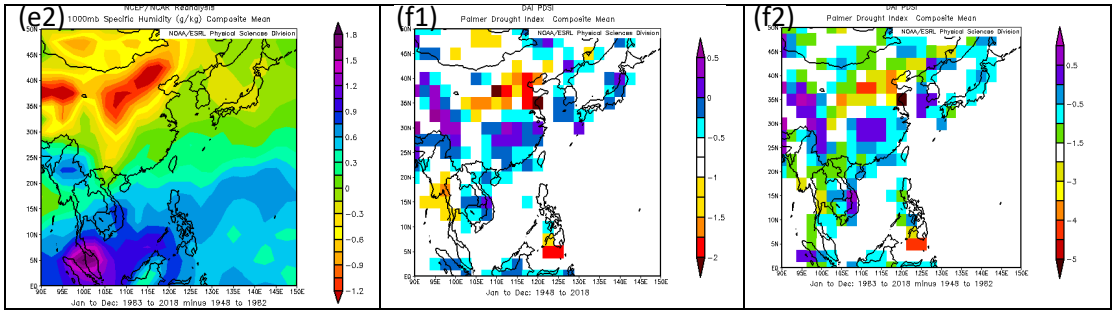

Figure 2 Mean/changes in annual (a1/a2) air temperature (ºC), (b1/b2) surface precipitable water (kg/m^2), (c1/c2) GPCP precipitation (mm/day), (d1/d2) Soil Moisture (mm), (e1/e2) Specific humidity (g/kg), and (f1/f2) Palmer Drought Severity Index of East Asia of 1948-2018 (between 1983-2018 and 1948-1982) based on NCEP-NCAR reanalysis data.

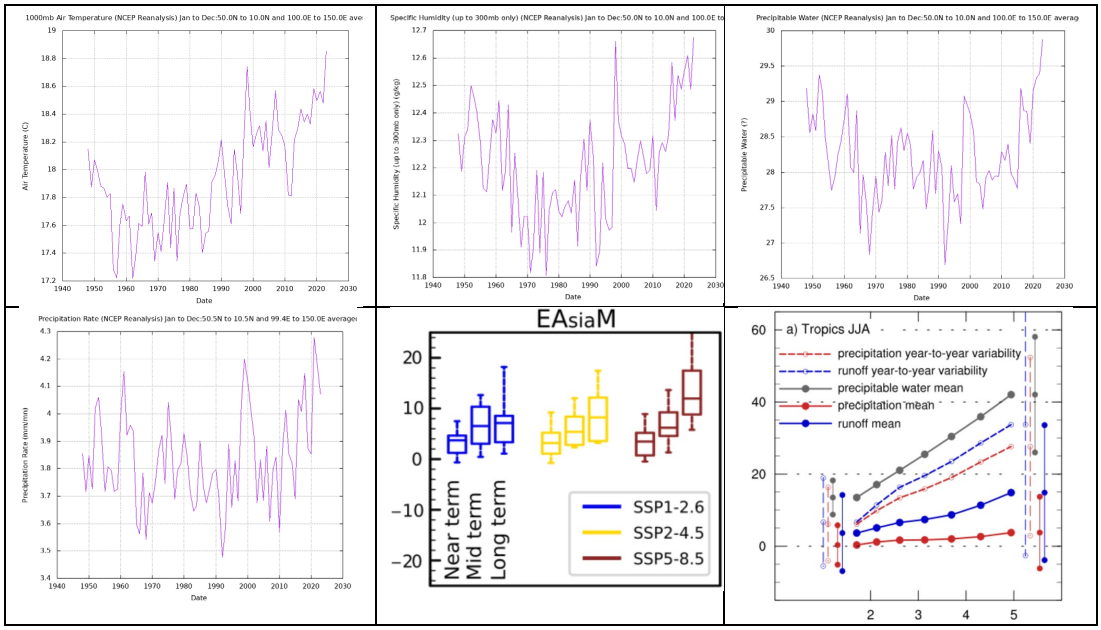

Figure 3 Changes of annual (a) air temperature, (b) specific humidity, (c) precipitable water and (d) precipitation rate of Japan of 1948-2022 using NCEP-NCAR reanalysis data; (e) % change in projected seasonal mean precipitation over regional monsoon domains for near-term (2021-2040), mid-term (2041-2060), and long-term (2081-2100) periods based on 24 CMIP6 models and three SSP scenarios (SSP1-2.6, SSP2-4.5 and SSP5-8.5); and (f) Relative change (%) in seasonal total precipitable water variability (green dashed line), precipitation (red dashed lines), runoff variability (blue dashed lines), as well as in standard deviation of precipitation (red solid lines) and runoff (blue solid lines) in summer (JJA) as a function of global-mean surface temperature for the CMIP6 multi-model mean across the SSP5-8.5 scenarios.

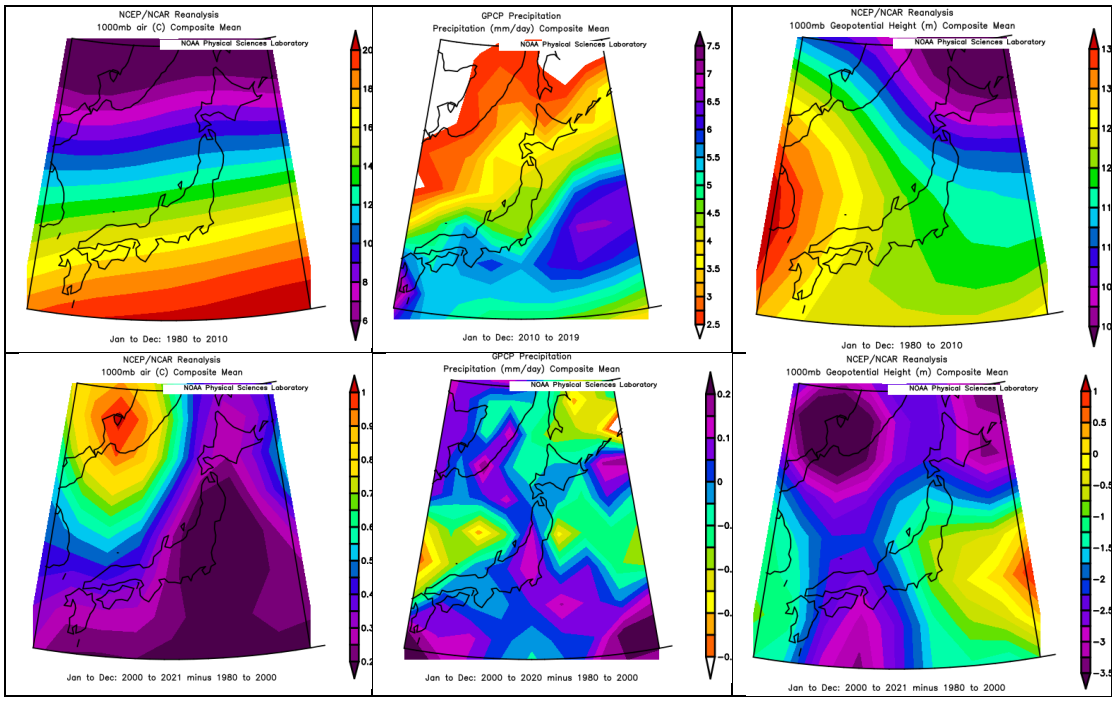

Figure 4 Annual air temperature, precipitation, and geopotential heights of Japan and the observed changes over 1980-2020 based on the NCEP reanalysis data.

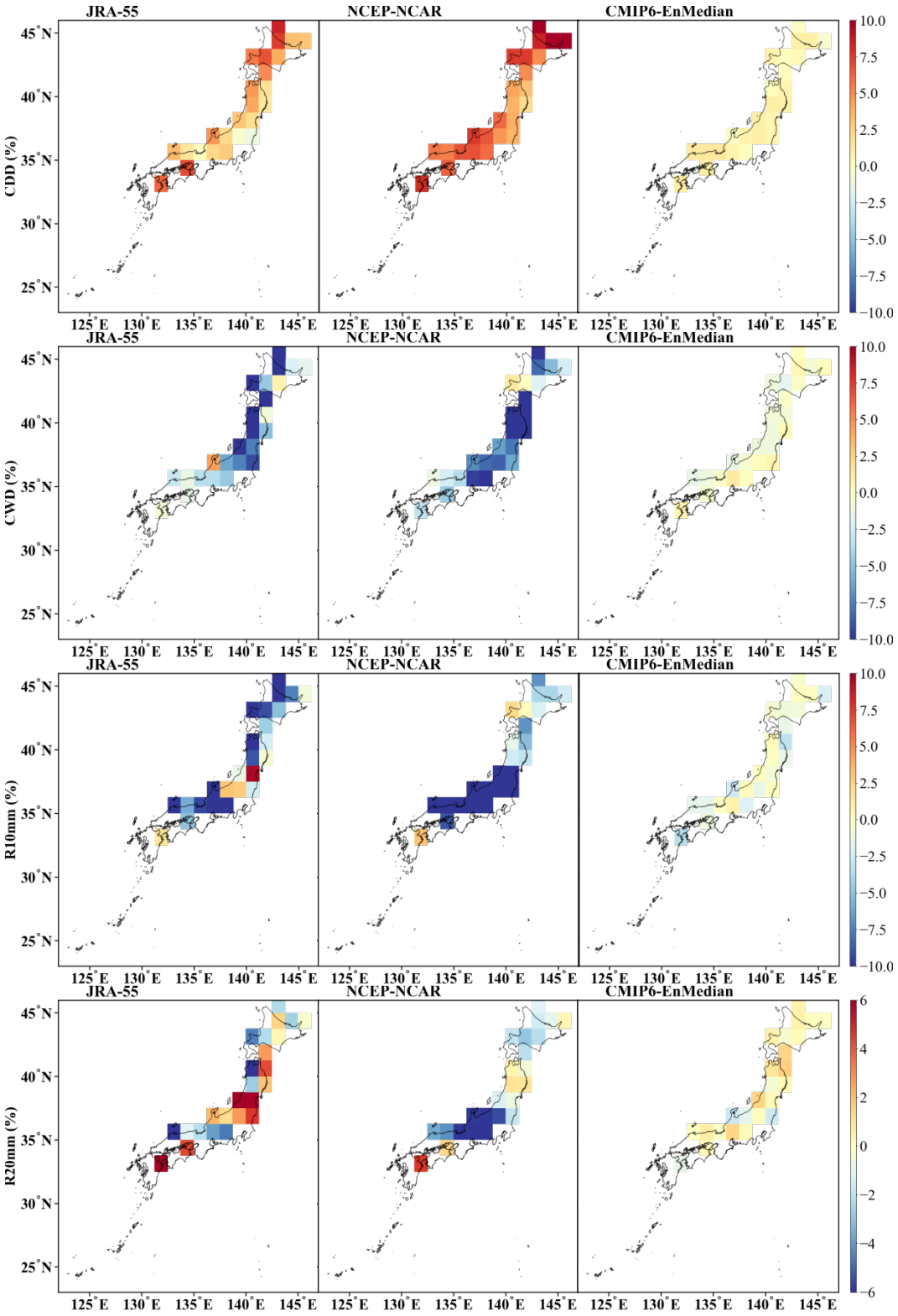
JRA-55
NCEP-NCAR
CMIP6-EnMedian
CDD (%)
CWD (%)
R10mm (%)
R20mm (%)
45°N
40°N
35°N
30°N
25°N
125°E
130°E
135°E
140°E
145°E
10.0
7.5
5.0
2.5
0.0
−2.5
−5.0
−7.5
−10.0
6
4
2
0
−2
−4
−6

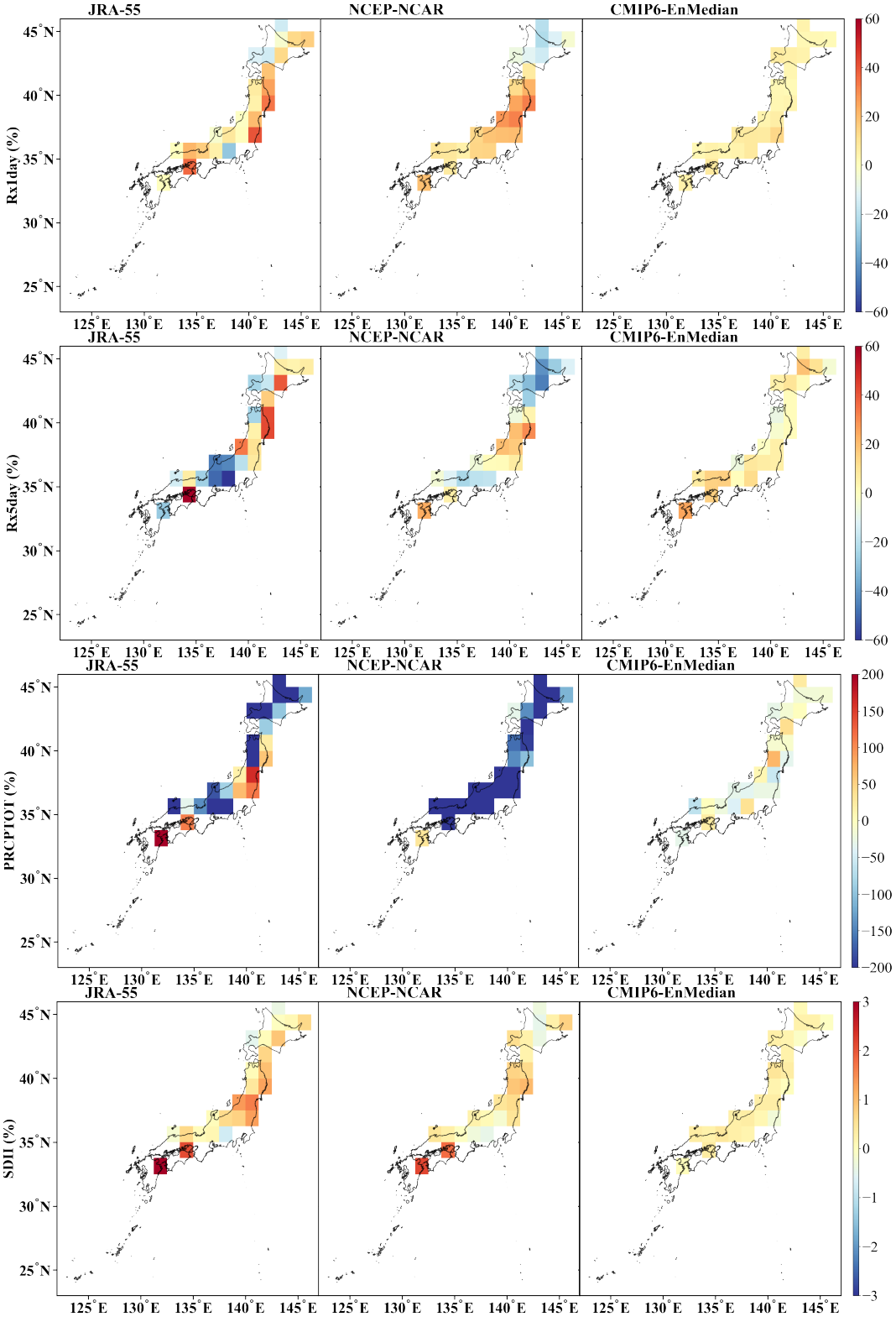
JRA-55
NCEP-NCAR
CMIP6-EnMedian
Rx1day (%)
Rx5day (%)
PRCPTOT (%)
SDII (%)
45°N
40°N
35°N
30°N
25°N
125°E
130°E
135°E
140°E
145°E
60
40
20
0
−20
−40
−60
200
150
100
50
0
−50
−100
−150
−200
3
2
1
0
−1
−2
−3

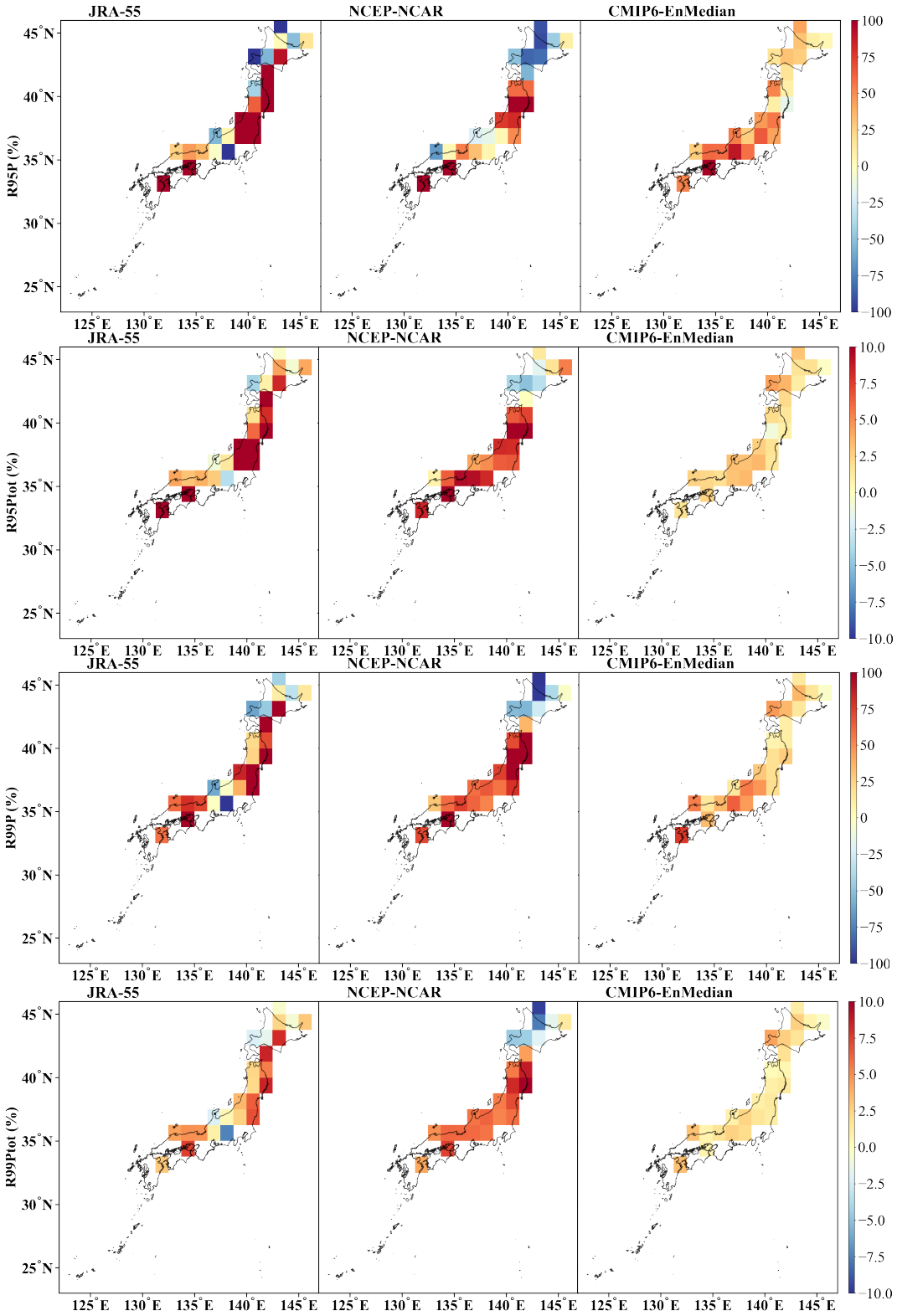
JRA-55
NCEP-NCAR
CMIP6-EnMedian
R95P (%)
R95Ptot (%)
R99P (%)
R99Ptot (%)
45°N
40°N
35°N
30°N
25°N
125°E
130°E
135°E
140°E
145°E
100
75
50
25
0
−25
−50
−75
−100
10.0
7.5
5.0
2.5
0.0
−2.5
−5.0
−7.5
−10.0

Figure 5 The percentage of linear trends of JRA-55 (left), NCEP-NCAR (middle) and CMIP6 Ensemble Median (CMIP6-EnMedian, right) for the 12 extreme precipitation indices over the 1958–2014 study period. Increasing and decreasing trends are shown in red and blue, respectively.

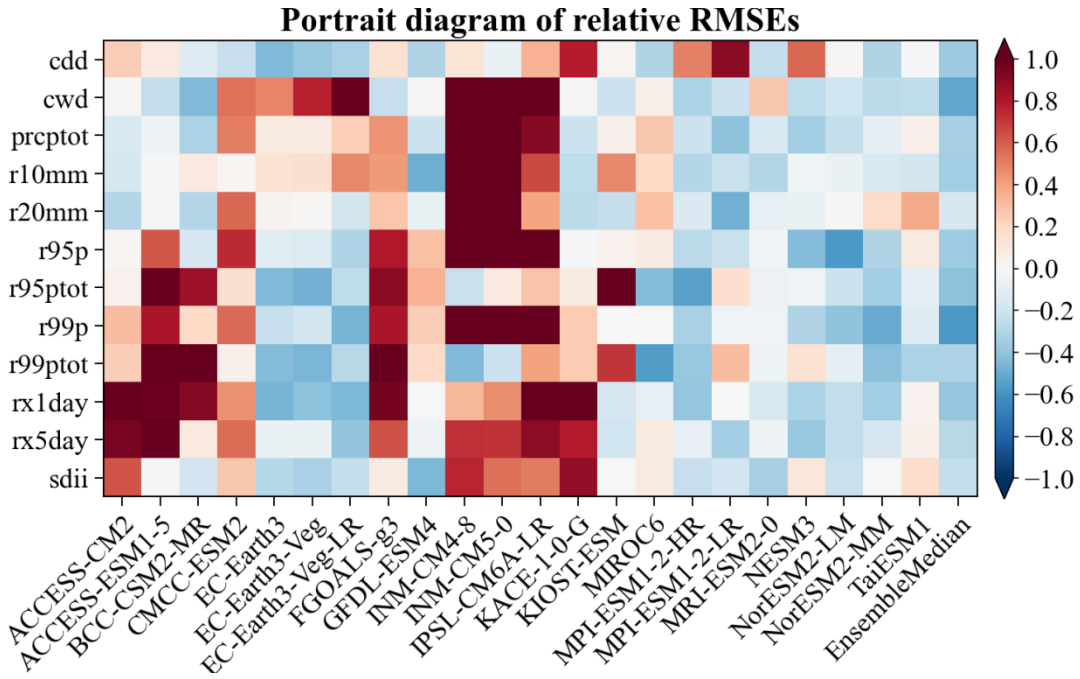

Figure 6 The "portrait" diagram of relative *RMSE'*$_{XY}$ for the 1981–2010 climatologies of twelve extreme precipitation indices of Japan simulated by the 22 CMIP6 models and the CMIP6 ensemble median (CMIP6-EnM) is placed on the rightmost column. The RMSEs are spatially averaged over all grid points of Japan. The relative RMSEs range from +1 (dark red) to -1 (dark blue).

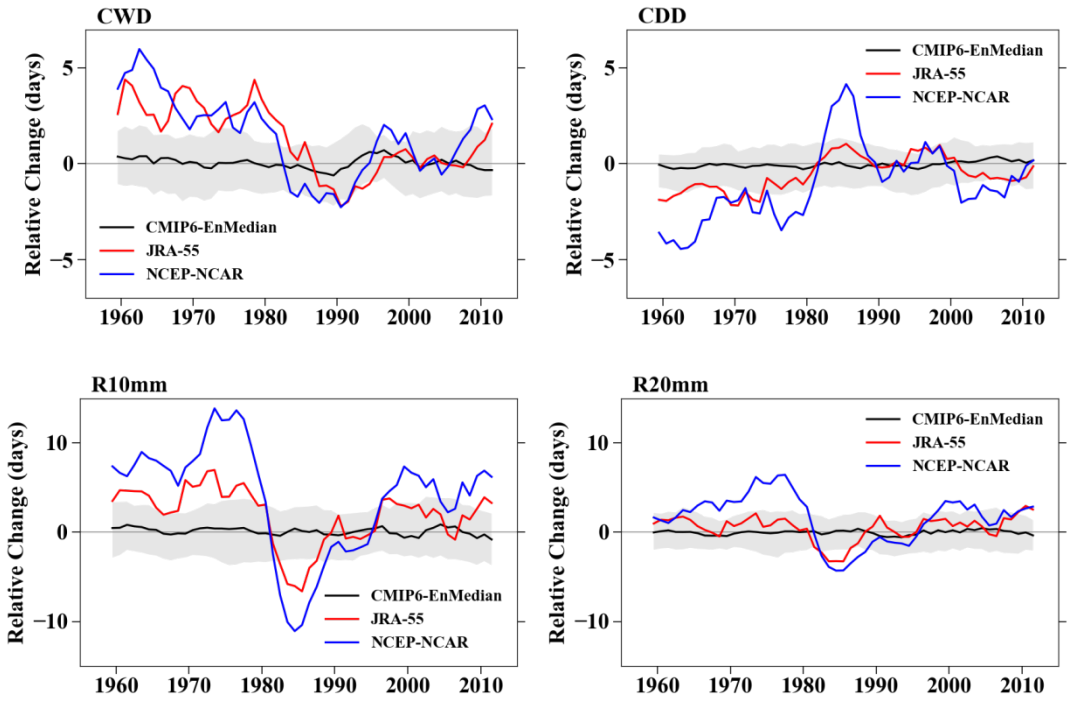

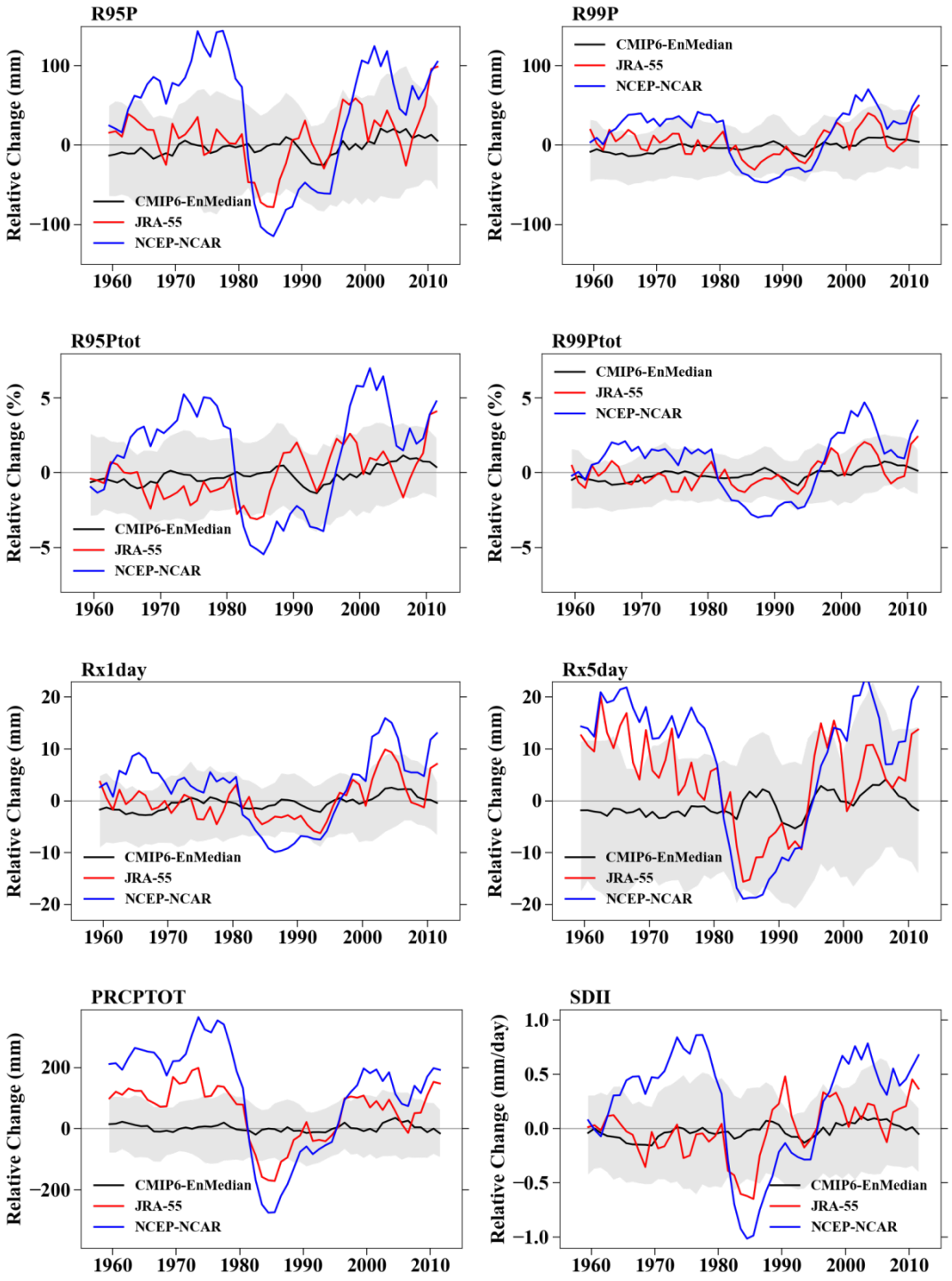

Figure 7 Temporal changes of 12 extreme precipitation indices anomalies over Japan estimated from JRA-55, NCEP-NCAR and the CMIP6 ensemble from 1958 to 2014 relative to 1981−2010. Solid lines indicate the results of JRA-55, NCEP-NCAR and CMIP6 Ensemble Median; shadings show the interquartile ensemble spread of 22 individual CMIP6 climate models (25th and 75th quantiles). Time series are smoothed with a 5-yr running mean filter from 1958 to 2014. A horizontal grey solid line passes through the time axis of 1958-2014.

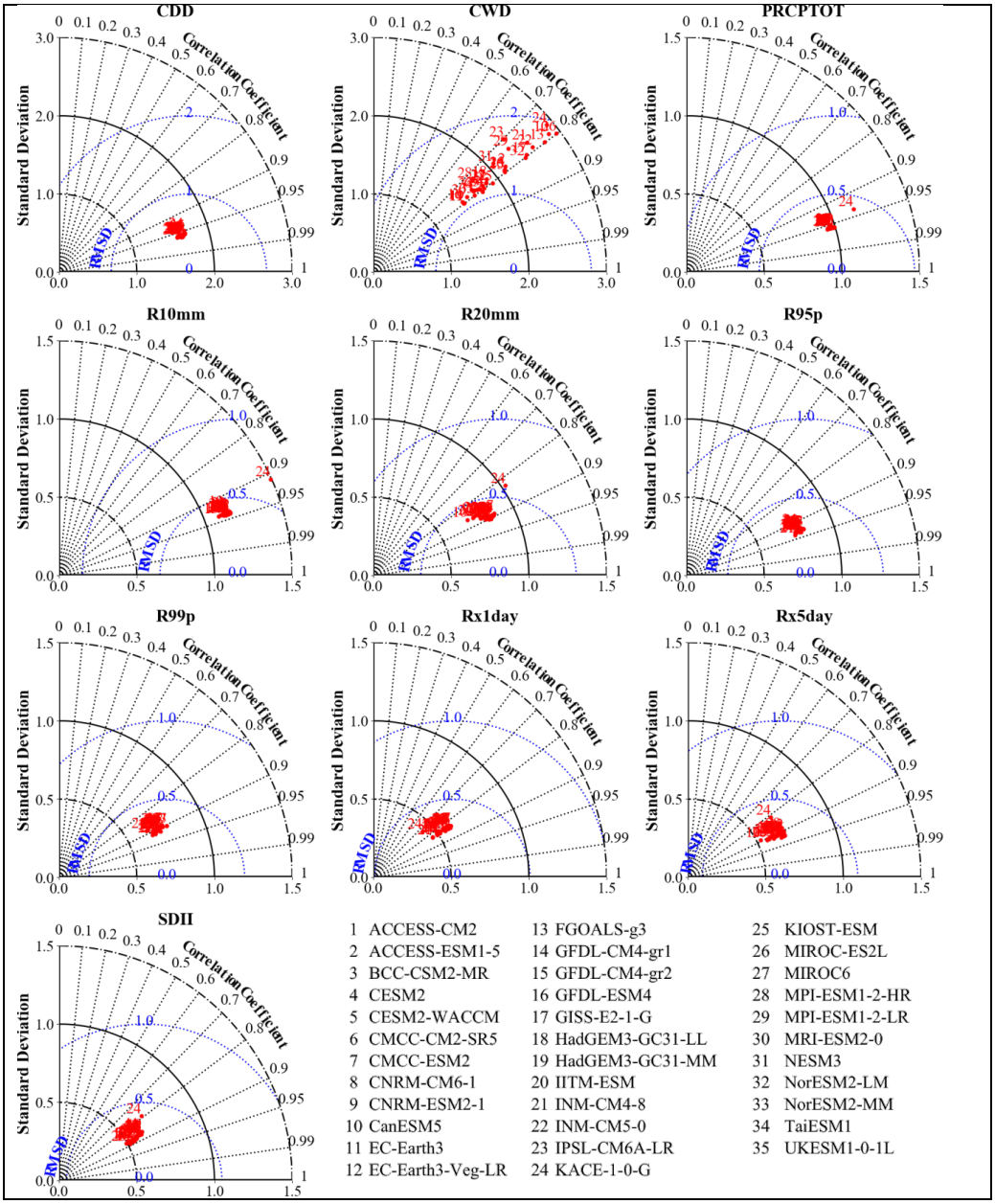

Figure 8 Taylor diagrams of ten extreme precipitation indices between observation and 35 CMIP6-GCMs over East Asia where angular axes show spatial correlations between modeled and observed fields while radial axes show spatial standard deviation (root-mean-square deviation) normalized against that of observations.

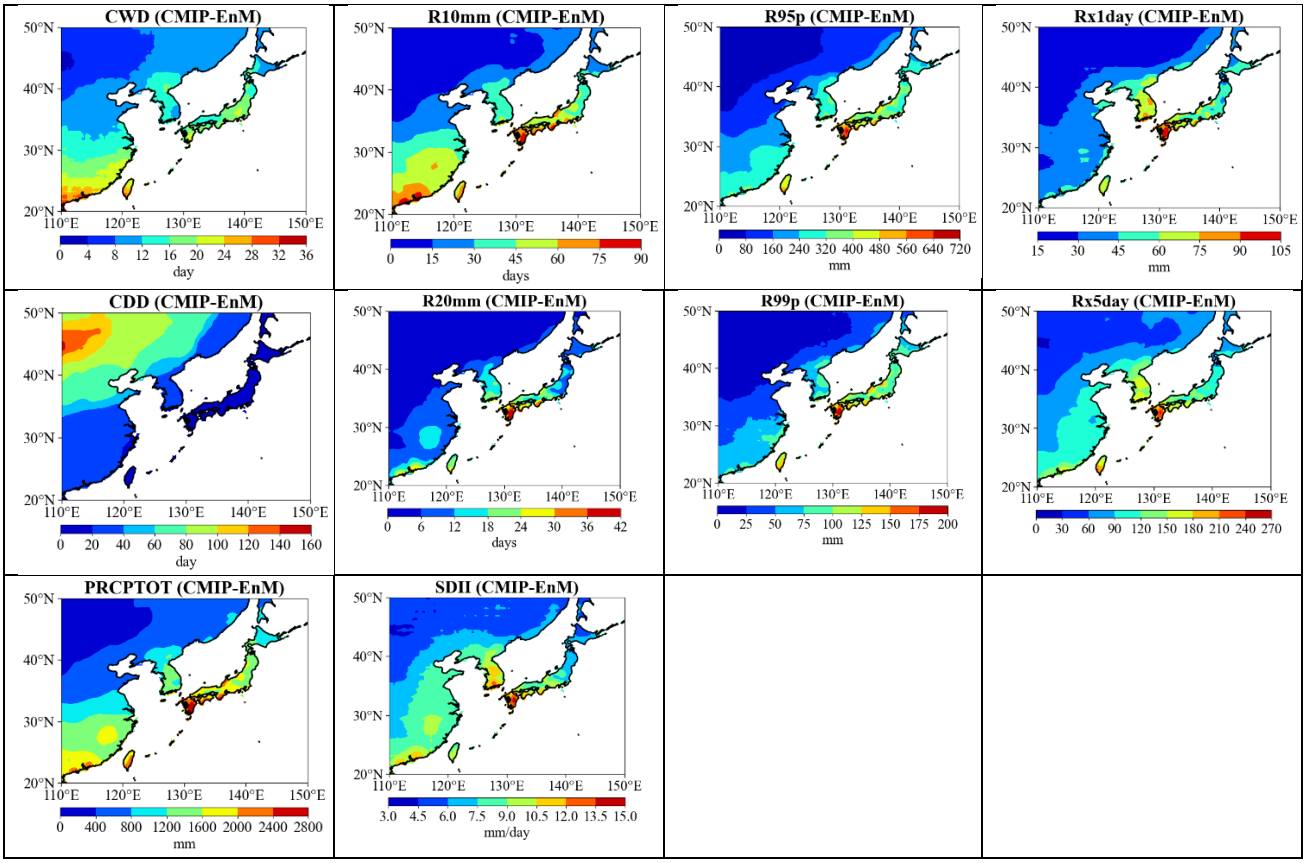

Figure 9 Spatial distributions of extreme precipitation indices over East Asia and Japan based on the ensemble median of CMIP6 GCMs' simulations for 1958-2014 (CMIP6-EnM).

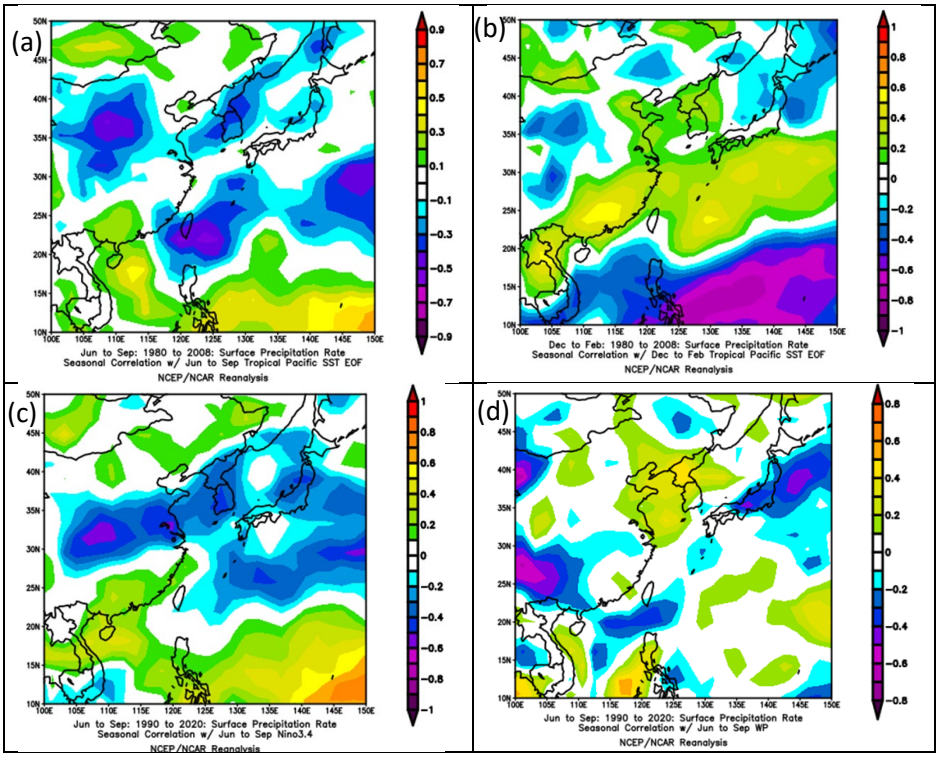

Figure 10 Limited correlation between (a) JJAS precipitation and (b) DJF precipitation of East Asia with the EOF of Tropical Pacific SST, and JJAS precipitation with (c) ENSO and (d) WP indices, respectively.

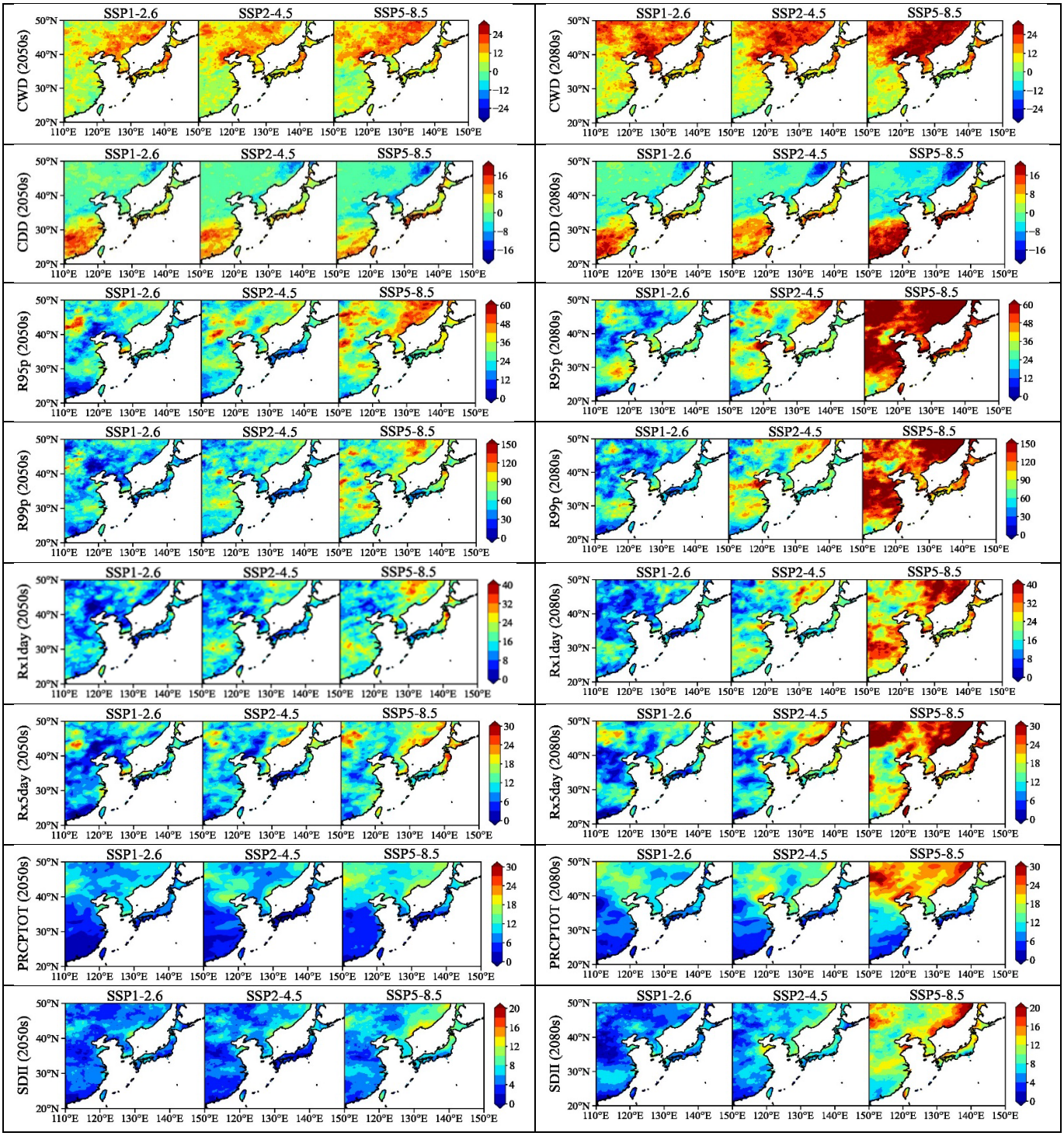

Figure 11 Ensemble medians of projected changes to CWD, CDD, R95p, R99p, Rx1day, Rx5day, PRCPTOT, and SDII of East Asia under SSP1-2.6, SSP2-4.5 and SSP5-8.5 climate scenarios of CMIP6 for the 2050s and 2080s.